Effects of Rate-sensitivity in Dynamically Loaded 3D Fracture Specimen

TOSHIO NAKAMURA
Department of Mechanical Engineering, State University of New York, Stony Brook, NY 11794, USA

ABSTRACT

Based on detailed finite element solutions, effects of rate-sensitivity on the crack tip fields of dynamically loaded 3D three-point-bend specimen are analyzed. The fracture toughness parameter of rate-dependent solid is found to be consistently lower than that of rate-independent solid under similar ligament loads. The variation of J through-thickness indicates that higher loading rate is likely to promote a more uniform advance of the crack front and brittle-like fracture characteristics in rate-dependent solid. Furthermore, in conjunction with the concept of transition time, the applicability of deep-crack J formula is studied.

1. INTRODUCTION

Several experimental procedures have been proposed for the measurement of dynamic fracture toughness. In the earlier study by Nakamura, Shih and Freund (1986b), a full-field 3D finite element analysis of a rate-independent three-point-bend bar was reported. The crack tip values of fracture toughness parameter, J, were computed by means of a three-dimensional domain integral expression, and the results were compared with the experimentally measurable J based on the deep-crack formula proposed by Rice, Paris and Merkle (1973). Furthermore, a notion of transition time was introduced to provide a practical bound on the time range over which conditions of J-dominance prevails near the crack front and the deep-crack formula is applicable under transient loadings. In the present study, a full-field three-dimensional finite element analysis of a dynamically loaded three-point-bend fracture specimen has been carried out to investigate the effects of loading rate and rate-sensitive plastic response on crack tip fields. The material properties chosen are representative of a high-strength low carbon steel subjected to high rates of loading.

The variation of local J along the crack front and its dependence on loading rate and elapsed time are particularly relevant to the interpretations of dynamic fracture data. Under high loading rates, the yield/flow stress of rate-dependent material is elevated. Thus, it is expected that at similar ligament loads, the plastic flow is smaller while the near tip stresses are higher as the loading rate increases. Significant crack growth tunneling has been observed in extensively yielded (quasi-statically loaded) test specimens of typical dimensions, and this has been explained by the large drop in J along the crack front as the free edge is approached. In the present analysis, the behavior of J across the crack front under various loading rates is carefully investigated for rate-dependent and rate-independent solids.

2. DYNAMIC J-INTEGRAL

2.1 Energy Integral for Dynamic 3D Crack Front

The J-integral is a useful parameter in characterizing crack tip fields. It is equivalent to the energy release rate and relates to the amplitude of a crack tip singularity field in an inelastic solid. A mathematical expression for the local energy release rate J in terms of near tip dynamic fields for three-dimensional bodies is

$$J_{\text{local}}(s) = \lim_{\Gamma \to 0} \mu_k(s) \int_\Gamma \left[(W+T)\, n_k - \sigma_{ij} n_j \frac{\partial u_i}{\partial x_k} \right] d\Gamma \ . \tag{1}$$

Here the subscript 'local' distinguishes J for a *pointwise* value along a three-dimensional crack front, and s is a parameter which represents the location of the crack tip on the crack front. A path Γ where the integral is evaluated surrounds the crack front at s and lies in the plane perpendicular to crack front. The unit vector $\mu_k(s)$ denotes the local direction of crack advance. Also W and T are the stress work and the kinetic energy densities, respectively, σ_{ij} and u_i are the cartesian components of stress and displacement, and n_i are the components of a unit vector normal to Γ and to the crack front tangent vector at s. The above integral defines a local energy release rate along any curvilinear crack front in 3D space.

From a discrete computational point of view, the expression (1) is not suitable for evaluating values of $J_{\text{local}}(s)$ since an accurate numerical evaluation of fields near the crack front is difficult. In the present analysis, an alternate form, the domain integral, is employed. In the domain integral method the local J is determined from the energy release due to virtual extension of a small crack front segment. With the aids of the equation of motion, the divergence theorem and weighting function q_k, the energy release of a crack front segment may be expressed in terms of volume/domain integral as,

$$\overline{J} = \int_{\text{segment}} q_l(s') \mu_l(s') J_{\text{local}}(s')\, ds' = \int_V \left[\sigma_{ij} \frac{\partial u_i}{\partial x_k} \frac{\partial q_k}{\partial x_j} - W \frac{\partial q_k}{\partial x_k} + \rho \frac{\partial^2 u_i}{\partial t^2} \frac{\partial u_i}{\partial x_k} q_k \right] dV \ . \tag{2}$$

Here the vector $q_l(s)$ equals the direction and magnitude of the virtual crack extension, V is a volume which encloses the segment and ρ is the material density. A simple approximation to J_{local} is obtained by assuming that it is nearly constant within such crack segment.

$$J_{\text{local}}(s) = \overline{J} \Big/ \int_{\text{segment}} \mu_k(s) q_k(s)\, ds \ . \tag{3}$$

Detail discussions of the domain integral method can be found in Nakamura, *et al.* (1986b) and Moran and Shih (1987).

2.2 Deep-Crack J Estimates for Transient Problems

On the basis of transient 2-D finite element analysis, a formula for the computation of dynamic J from measurable quantities was proposed by Nakamura, *et al.* (1986a). The formula is a modified version of a deep-crack formula for calculating the value of J under essentially equilibrium conditions (Rice, *et al.*, 1973). Under dynamic loading, the inertial resistance of the specimen screens the crack tip region from the applied loads. To minimize this effect, the variables in the quasi-static formula are replaced by equivalent variables which characterize the near crack region of the body. Thus the moment is taken to be the net moment M_L carried by the ligament, and the corresponding rotation is replaced by the crack mouth opening displacement divided by the distance between the crack mouth and the hinge axis on the ligament. With these changes, the formula,

$$J_{\text{measurable}}(t) = \frac{2}{bB} \int_0^{\theta(t)} M_L(t')\, d\theta(t') \ , \tag{4}$$

was proposed for estimating the value of J in a dynamically loaded three-point-bend ductile fracture specimen. In the above expression, b is the ligament length, B is the specimen thickness and θ is the rotation of cracked section. At the level of beam approximation, the integral of the moment and angle in (4) represents the work done on the ligament. In view toward the experimental testing, suitable methods and surface locations for measurements of moment and rotation are discussed in Nakamura, *et al.* (1986a,b).

3. FINITE ELEMENT ANALYSIS

3.1 Computational Model

The relative dimensions of the three-point-bend specimen are $L/H = 2.0$, $a/H = 0.5$, $B/H = 0.5$ and $L_T/H = 2.25$ where H is the width of the specimen, L is the length between the cracked section and the remote support, a is the crack length, B is the thickness and L_T is the half-length of the specimen (see Fig. 1(a)). These relative dimensions are in accord with ASTM specifications for the specimen for quasi-static fracture toughness evaluation. In the present analysis, the width H is set equal to 2 inches (0.0508 m).

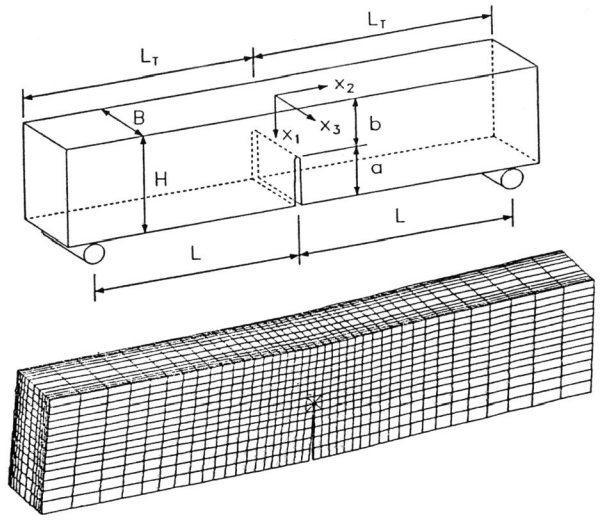

Fig. 1 (a) Schematic of three-point-bend specimen. The coordinates x_1, x_2 and x_3 are indicated. (b) Deformed finite element model.

Only a quarter of the three-point-bend specimen (region $x_2 \geq 0$, $x_3 \geq 0$) is modeled since the problem possesses reflective symmetry with respect to the crack plane ($x_2 = 0$) and the mid-plane ($x_3 = 0$). A deformed finite element model of the specimen constructed with 8-node trilinear hexahedron (brick) elements is shown in Fig. 1(b). The six layer of elements through half-thickness are bounded by the planes $x_3/B = 0.0,\ 0.17,\ 0.27,\ 0.35,\ 0.41,\ 0.46,\ 0.5$. The crack front is surrounded by six rings of specially arranged crack-tip elements. Each ring contains four brick elements which are collapsed into wedges. The quarter-mesh has a total of 1692 elements (282 elements on each layer) and 2233 nodes.

On the plane of the uncracked ligament and the mid-plane, normal displacements are prescribed to vanish. The model is roller-supported along the line $x_1 = H$, $x_2 = L$. A uniform pressure is

applied over a quarter-region bounded by $0 \le x_2 \le H/8$ and $0 \le x_3 \le B/2$ on the plane $x_1 = 0$ so that the quarter-load is $P/4$. Twelve element surfaces constitute the plane of contact.

The material model follows the strain hardening elastic visco-plastic theory. The total strain rate is composed of elastic and visco-plastic parts, and under uniaxial loading condition, they are

$$\dot{\epsilon}_e = \frac{\dot{\sigma}}{E}\,, \qquad \text{and} \qquad \dot{\epsilon}_{vp} = \beta \left[\frac{\sigma}{f(\epsilon)} - 1\right]^m \quad \text{for} \quad \sigma > f(\epsilon)\,, \tag{5}$$

where E is Young's modulus, β is fluidity parameter and m is overstress parameter. The function $f(\epsilon)$ corresponds to strain hardening and given by $f(\epsilon) = \sigma_o\,(\epsilon/\epsilon_o)^{1/n}$. Here σ_o and ϵ_o are the static yield stress and strain for rate-independent limit ($\beta \to \infty$) and n is the strain hardening exponent. The material parameters are chosen so that they are representative of low strain hardening cold-rolled carbon steel (Brickstad, 1983). For the rate-dependent model we tested, they are $E = 200\,\mathrm{GN/m^2}$, $\nu = 0.3$, $\rho = 7800\,\mathrm{kg/m^3}$, $\sigma_o = 1485\,\mathrm{MN/m^2}$, $\beta = 4100\,/\mathrm{s}$, $m = 2$ and $n = 10$. The rate-independent solid model has the same values except the fluidity parameter is set $\beta \to \infty$.

3.2 Dynamic Analysis

Two cases of load history are considered. In the case of *higher loading rate*, the load, applied at the tup (mid-span of the specimen), is increased with the initial loading rate of $p = (PL/2M_o)/(tc_1/H) = .15$ (c_1 is the longitudinal wave speed). The load level is kept constant after it reaches $PL/2M_o = 1.2$ (see insert in Fig. 2). For the *lower loading rate* case, the initial loading rate is set at $p = .03$. The maximum load level is again kept at $PL/2M_o = 1.2$. Each loading rate is tested in the rate-dependent ($\beta = 4100\,/s$) and rate-independent ($\beta \to \infty$) computations. These loading rates approximately represent load application rates that have been observed in drop-tower three-point-bend bar fracture experiments through the use of impact absorber material.

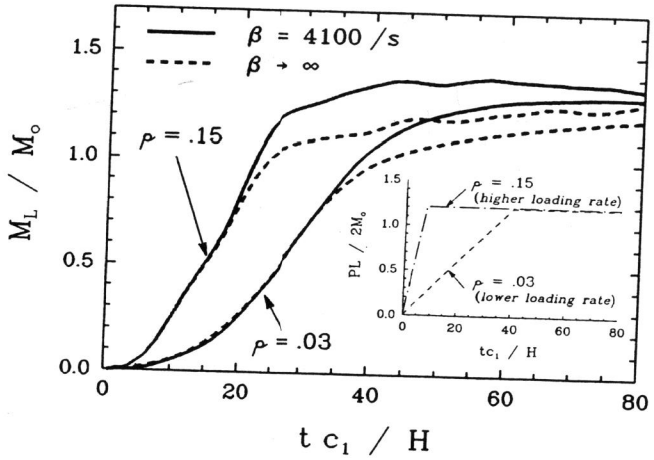

Fig. 2 Moment carried by ligament plane *vs.* elapsed time for rate-dependent ($\beta = 4100\,/s$) and rate-independent ($\beta \to \infty$) solids. Applied load history at tup for higher ($p = .15$) and lower ($p = .03$) initial loading rates is shown in insert.

The actual moment carried by the ligament M_L is normalized by the limit moment given by

the plane strain rigid-perfectly plastic analysis (Green and Hundy, 1956). The limit moment, M_o has the value $0.364\,\sigma_o b^2 B$ where b is the ligament length. Plotted in Fig. 2 are the increase of the normalized moment M_L/M_o with dimensionless elapsed time $t\,c_1/H$ for rate-dependent and rate-independent solids under two different initial loading rates. While the response of the specimen is primary elastic ($M_L/M_o < 0.8$), two curves are nearly identical under each loading condition. At higher level of load, however, moment becomes larger in rate-dependent solid at respective elapsed time. More gradual increase of moment in rate-independent solid can be explained by greater energy dissipation through plastic flow. In fact, although quantitatively different, the trend of rate-dependent result follows closer to the result of a linear elastic solid.

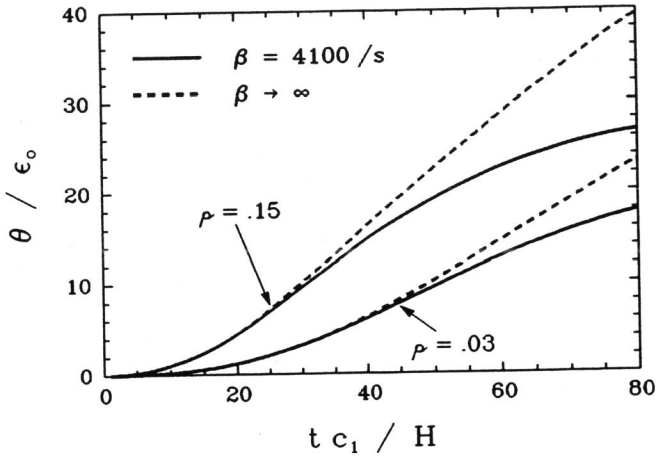

Fig. 3 Rotation of cracked section plotted *vs.* normalized time.

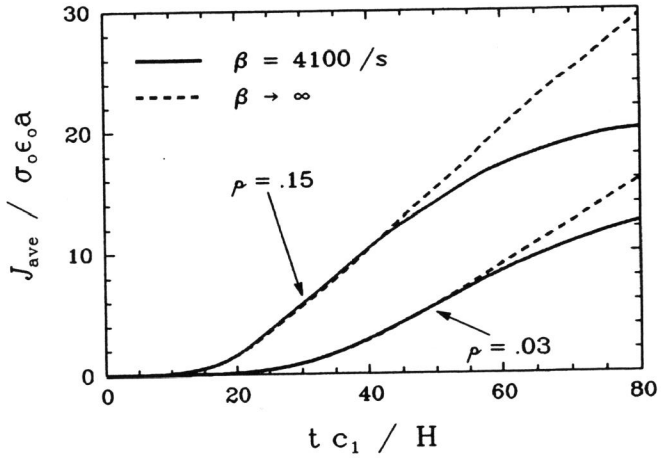

Fig. 4 Average J over entire crack front plotted *vs.* normalized time.

The rotation of the cracked section θ as a function of time is shown in Fig. 3. Again the discrepancy in the two solids is negligible while the specimen remain primary elastic. For $\theta/\epsilon_o > 8$, the rotation of the rate-independent solid is increasing at faster rate. At first glance, this result seems unexpected, since the corresponding moment carried by the ligament is consistently *lower* than that of rate-dependent solid! However this can be explained by substantially smaller plastic deformation in rate-dependent solid due to elevated flow stress under high loading rate. At the element nearest to the crack front, the plastic strain rate of the rate-independent solid reaches twice as large as that of rate-dependent solid under higher loading rate.

The J_{local} along crack front nodes are obtained from finite element fields using the domain integral method. The arc-length weighted average value is denoted as J_{ave}. The increase of $J_{\text{ave}}/\sigma_o\epsilon_o a$ with time $t\,c_1/H$ is plotted in Fig. 4. The trends of the two solids under each loading rate are very similar to the one shown by the rotation of cracked plane. The J_{ave} in rate-independent solid increases at nearly constant rate while the rate-dependent results start to level off at larger $t\,c_1/H$.

Shown in Fig. 5 is the distribution of J along crack front for $p = .15$ at the transition time, t_T. The transition time is determined from the ratio of total kinetic energy and the total deformation energy (see discussion in Nakamura, *et al.*, 1986a). The transition time is a function of Young's modulus and the geometry of model. It also depends slightly on the loading rate, but it is essentially independent of rate-sensitivity of material. The figure shows familiar variation of J_{local}, the maximum at the mid-plane ($x_3/t = 0$) and the minimum at the edge-plane ($x_3/t = 0.5$). At $t_T c_1/H = 25$, the through-thickness variations of rate-independent solid is somewhat greater, indicating larger plastic flow. Thus, the rate-sensitivity tend to suppress the increasing crack front variation of J under higher load level.

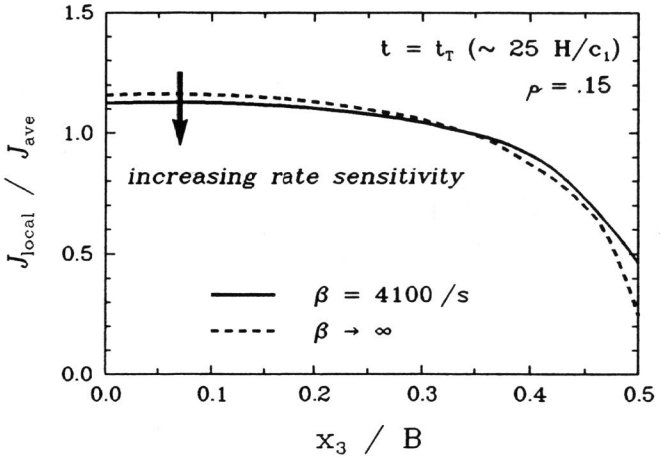

Fig. 5 Local J, at transition time, normalized by average J plotted *vs.* position along crack front.

The degree of J variation through-thickness as function of average J is illustrated in Fig. 6. Here the degree of J variation, $\Delta J/J_{\text{ave}}$, is defined as the normalized difference between J_{local} at the mid-plane and the edge-plane (two extreme values). The value $\Delta J/J_{\text{ave}} \simeq 0.2$ at $J_{\text{ave}}/\sigma_o\epsilon_o a \to 0$ corresponds to the linear elastic solution. In the figure, the degree of variation of rate-dependent solid ($\beta = 4100\ /s$) is consistently lower than that of rate-independent solid ($\beta \to \infty$). With rate-independent solid, the degree of J variation as a function of J_{ave} is *invariant* to the loading rate. In fact, the degree of J variation at the quasi-static limit ($p \to 0$), with either rate-independent or rate-dependent solid, shows nearly identical result. Thus, it is clearly that greater crack

front J variation for a given J_{ave} is achieved for less rate-sensitivity of material and under lower loading rate. Alternatively, if J may be adopted as a fracture characterizing parameter, more uniform crack front advance can be predicted under higher loading rate or in more rate-sensitive material.

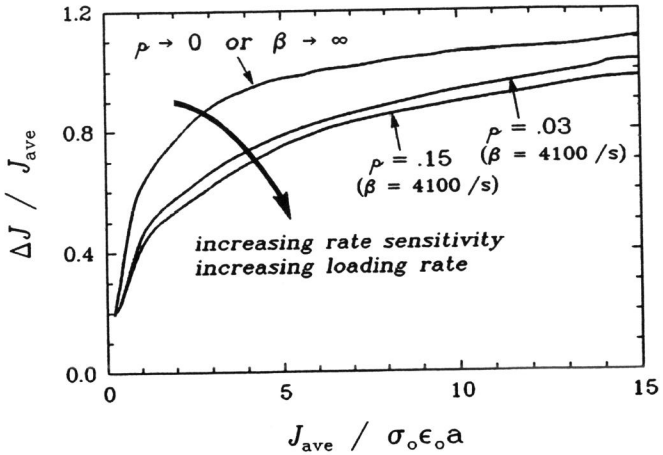

Fig. 6 Degree of J variation through-thickness plotted *vs.* average J. Larger rate sensitivity and higher loading rate promote smaller variation.

3.3 Comparison of (Actual) J and Measurable J

With the moment (Fig. 2) and the rotation (Fig. 3) as input parameters in (4), the value of $J_{\text{measurable}}$ is obtained for each of rate-dependent and rate-independent solid. In Fig. 7, $J_{\text{measurable}}$ normalized by the actual J (1) (Fig. 4) is plotted for the case of $p = .15$. While elastic response dominates, the difference in the two results is minimal. During the *short time* period, $t < t_T$, the field near crack has not been stabilized, and thus, the existence of J-dominated field is unlikely. In addition, accurate evaluation of J based on (4) is not possible as can be observed from the figure. The ratio is substantially larger than unity, then falls below and starts to increase monotonically at about the transition time. At the *long time* period, $t > t_T$, the response of specimen is dominated by the deformation energy, and $J_{\text{measurable}}$ shows steady improvement. These trends are consistent in the results of both materials. Thus, in order to determine J from measurable quantities, fracture initiation must occur some time after t_T, regardless of material rate-sensitivity. At $t\,c_1/H > 60$ the ratio continues to overshoot in the case of rate-dependent solid. This may be due to slight (ligament moment) unloading occurring at $t\,c_1/H > 60$ with rate-dependent solid (see Fig. 2).

The results presented here have shown various aspects of rate-sensitivity on the fracture specimen subjected to dynamically loaded condition. We have observed, quantitatively, effects of loading rate on the J variations through-thickness in rate-dependent solid. If the fracture toughness of rate-dependent solid is nearly independent of loading conditions, then more uniform crack front advance can be expected under higher loading rate. The accuracy of the deep-crack formula is also investigated, and the formula is shown to be applicable in dynamically loaded rate-dependent specimen. In addition, transition time is proven to be a useful parameter in dynamic fracture analysis with rate-dependent materials as well as with rate-independent materials. Based on the types of loading history considered here, there is a tendency for elastic

unloading to occur within the crack front field with rate-dependent solid. This must be carefully regarded in dynamically load fracture testing of rate-sensitive materials.

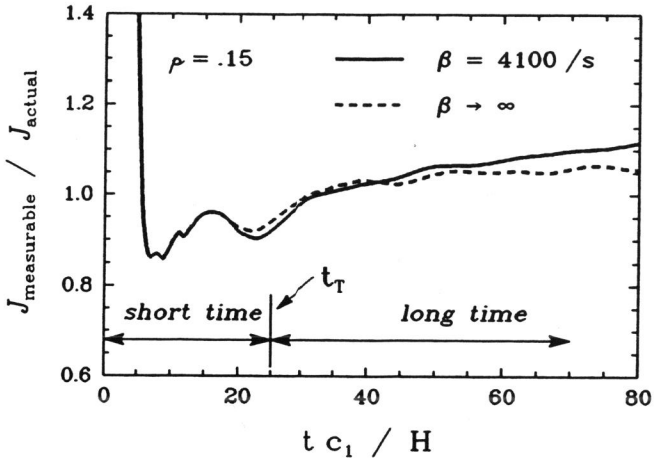

Fig. 7 Normalized measurable J, under higher loading rate, plotted *vs.* time. The transition time and ranges for short time and long time are indicated.

ACKNOWLEDGEMENT

The author gratefully acknowledge the technical discussions with Professor C. F. Shih. The computations were performed on VAX 8600 at Department of Mechanical Engineering, S.U.N.Y. at Stony Brook, and at the John von Neumann Center, Princeton.

REFERENCES

Brickstad, B. (1983). A viscoplastic analysis of rapid crack propagation experiments in steel. *J. Mech. Phys. Solids*, 31, 307-327.

Green, A. P. and B. B. Hundy (1956). Initial plastic yielding in notch bend tests. *J. Mech. Phys. Solids*, 4, 128-144.

Moran, B. and C. F. Shih (1987). Crack tip and associated domain integrals from momentum and energy balance. *Eng. Fract. Mech.*, 27, 615-642.

Nakamura, T., C. F. Shih and L. B. Freund (1986a). Analysis of a dynamically loaded three-point-bend ductile fracture specimen. *Eng. Fract. Mech.*, 25, 323 - 339.

Nakamura, T., C. F. Shih and L. B. Freund (1986b). Three-dimensional transient analysis of a dynamically loaded three-point-bend ductile fracture specimen. *Brown University Report*, to appear in ASTM STP.

Rice, J. R., P. C. Paris and J. G. Merkle (1973). Some further results of J-integral analysis and estimates. *Progress in flaw growth and fracture toughness testing*, ASTM STP 536, 231-245.